Vector Field Decompositions Using Multiscale Poisson Kernel

Harsh Bhatia, Robert M. Kirby, *Senior Member, IEEE*, Valerio Pascucci, and Peer-Timo Bremer

Abstract—Extraction of multiscale features using scale-space is one of the fundamental approaches to analyze scalar fields. However, similar techniques for vector fields are much less common, even though it is well known that, for example, turbulent flows contain cascades of nested vortices at different scales. The challenge is that the ideas related to scale-space are based upon iteratively smoothing the data to extract features at progressively larger scale, making it difficult to extract overlapping features. Instead, we consider spatial regions of influence in vector fields as scale, and introduce a new approach for the multiscale analysis of vector fields. Rather than smoothing the flow, we use the natural Helmholtz-Hodge decomposition to split it into small-scale and large-scale components using progressively larger neighborhoods. Our approach creates a natural separation of features by extracting local flow behavior, for example, a small vortex, from large-scale effects, for example, a background flow. We demonstrate our technique on large-scale, turbulent flows, and show multiscale features that cannot be extracted using state-of-the-art techniques.

Index Terms—Helmholtz-Hodge decomposition, flow analysis, multiscale features

1 Introduction

Multiscale representations and the notion of scale-space analysis have long been a crucial building block of data analysis and signal processing. The fundamental idea is to split a signal into its *spectral components*, i.e., low versus high frequencies, in order to remove noise or analyze phenomena at different spatial or temporal *scales*, e.g., daily versus monthly versus seasonal temperature fluctuations. However, these techniques have been predominantly designed for scalar-valued signals, and applying them to vector fields is challenging. Turbulent flows, in particular, are known to contain features on a wide (and continuous) spectrum of scales [1]. Although scientists observe coherent structures at various temporal and spatial scales in animations, defining and extracting such features directly from a velocity field has proven elusive. Often, smoothing is applied to individual vector components or derived scalars, which can produce significant artifacts (see, e.g., Figs. 4 and 5).

We contend that multiscale flow features require a conceptually different viewpoint compared to conventional scale-space approaches, which consider a signal exclusively in terms of its frequency content, and use "scale" only to define the frequency range of the corresponding filter. In flow fields, however, one is often interested in global effects, e.g., the presence of a background flow or other large-scale motions, compared to local ones, e.g., small-scale vortices. These concepts are only loosely coupled to the frequency of the signal, but rather are more concretely defined in terms of spatial scales, and echo a Lagrangian viewpoint that distinguishes a local observer moving with the flow from a global one.

To create "observers" at different scales, we propose to extend Helmholtz's perspective [2], [3], according to which the flow at a given point is affected by the flow at every other point in the domain. Through this perspective, we propose to create different scales by explicitly restricting the region of influence for every point. In particular, using the natural Helmholtz-Hodge decomposition [4], [5], we split the flow into small-scale effects, i.e., induced by the flow within the region of influence, and large-scale effects, i.e., induced by flow structure further away. By continuously adjusting the filter size, we can create a multiscale decomposition based on *splitting* the observed effects, rather than *smoothing* signals. More importantly, the resulting decomposition has a physical interpretation: the large-scale flow describes the overall motion at a given scale, whereas the small-scale flow defines the relative motion as observed when moving with the large-scale flow. In the limit of an infinitesimal filter, the small-scale flow reverts to the traditional Lagrangian frame of reference, where the observer moves along particles in the flow.

Multiscale techniques, in general, create an alternate function to represent behavior above or below a chosen scale. Similarly, our approach creates alternate (small- and large-scale) vector fields, which can be analyzed using any of the existing vector field techniques. Our multiscale decomposition is not aimed at any specific type(s) of features. Rather, feature extraction can be seen as operations defined on vector fields, and our decomposition supports all known operations. This paper demonstrates computation of critical points, streamlines, and pathlines as operations on the derived field, which appear to identify interesting

- *H. Bhatia and P.-T. Bremer are with the Center for Applied Scientific Computing at Lawrence Livermore National Laboratory (LLNL), Livermore, CA 94550 USA. E-mail: {hbhatia, ptbremer}@llnl.gov.*
- *R.M. Kirby and V. Pascucci are with the Scientific Computing and Imaging Institute, University of Utah, Salt Lake City, UT 84112 USA. E-mail: {kirby, pascucci}@sci.utah.edu.*

Manuscript received 9 May 2019; revised 7 Mar. 2020; accepted 13 Mar. 2020. Date of publication 2 Apr. 2020; date of current version 29 July 2021. (Corresponding author: Harsh Bhatia.)
Recommended for acceptance by I. Hotz.
Digital Object Identifier no. 10.1109/TVCG.2020.2984413

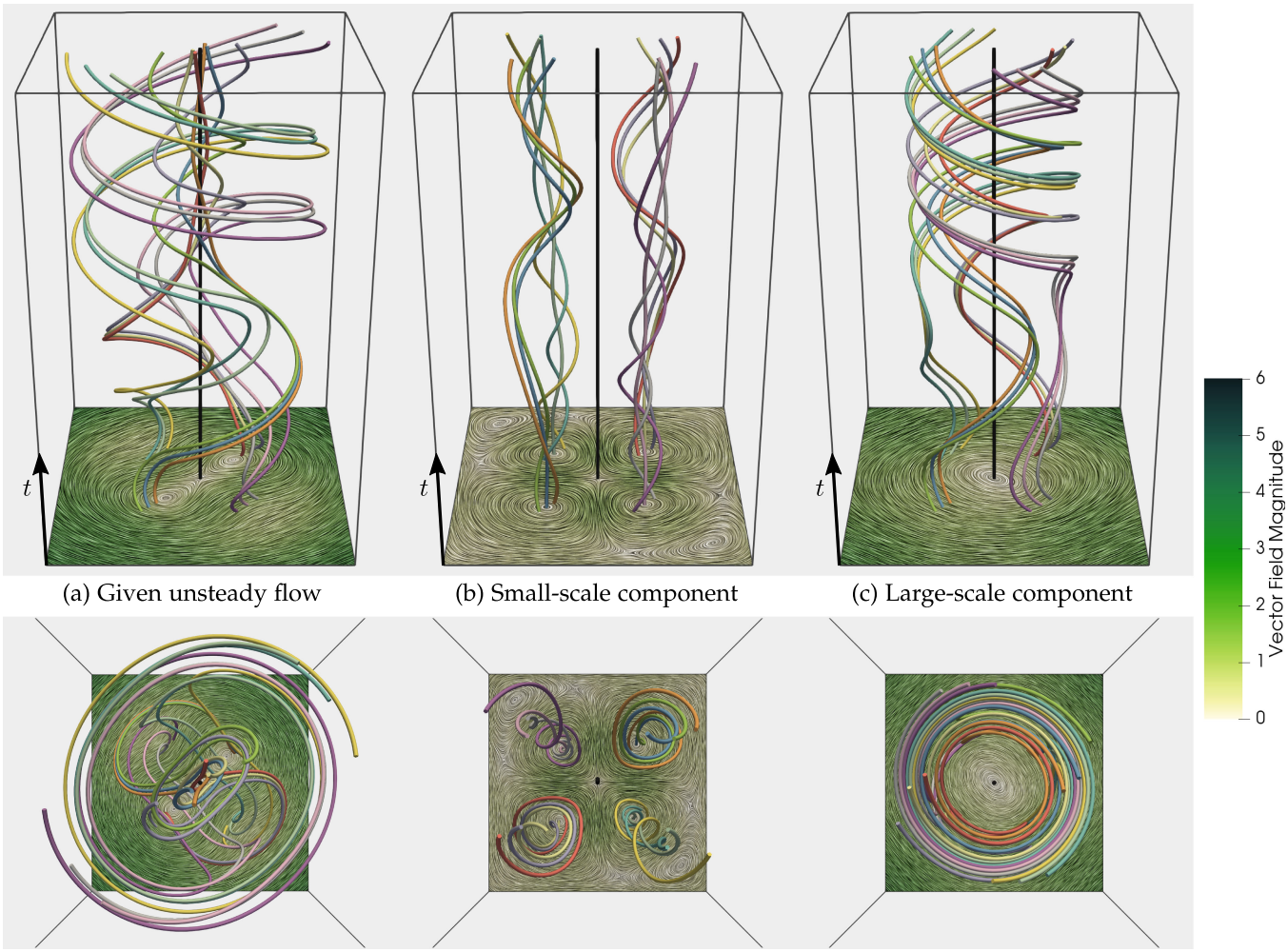

Fig. 1. Turbulent flows often exhibit complex phenomena at a wide range of spatial and temporal scales, and extracting multiscale features of interest is challenging. Here, we present a new framework for multiscale decomposition of flow fields. Using a novel splitting kernel, we decompose a given flow into a small-scale and a large-scale component (with respect to a chosen scale). The figure shows a synthetic flow (a), which comprises of a steady flow with four centers of rotation superimposed with a time-varying rotational flow (see Section 4.3). As seen in the figure, the superposition suppresses two of the centers and forces the other two inwards. Pathlines seeded near the expected vortices do not highlight swirling behavior. Our approach allows separating the flow features at the two scales, such that the small-scale flow component (b) captures the expected, stationary centers of rotation, whereas the large-scale component (c) captures the larger, time-varying rotation. The top view (bottom row) of the three flows highlights the difference in the spatial scales of (b) and (c), which are superimposed in the original flow (a).

phenomena even though they are not directly connected to their conceptual counterparts in the original flow.

Unlike existing approaches, the presented decomposition does not define "scale" using spectral content, but as the (spatial) region of influence. Here, we present a way to split the features based on the size of their region of influence. The splitting operation presented here depends entirely upon the spatial derivatives of the flow in spatial neighborhoods and, therefore, separates spatially multiscale features, such as multiscale vortices. Given a temporally smooth unsteady flow, the presented approach can be applied to each time-step independently, producing a decomposition that is multiscale in space and smooth in time. Particle paths in turbulent unsteady flows are typically affected by behavior at many scales, e.g., small vortical motion revolving in a larger vortex. As mentioned above, the goal is not to extract the particle paths of a given unsteady flow. Instead, our approach decomposes the flow and can represent the particle paths in the absence of large- or small-scale behavior. Considering that pathline computation, as an operation, is not linear, the presented decomposition provides a new way to separate the particle behavior with respect to flow at different scales (see Fig. 1).

Contributions. We present a new *multiscale decomposition* framework for vector fields. More specifically,

- We propose a new filter to solve the Poisson equation directly at multiscale. The proposed filter, a *modified Green's function*, is based on the idea of "splitting" local versus nonlocal effects, compared to the traditional "smoothing" filters.
- Using the modified Green's function, we extract multiscale features from vector fields. Our approach generalizes a recent work [5], which compensates for the global harmonic background flow, by allowing compensation for for more general types of flows.
- We present a Fourier-based approach to compute the multiscale decomposition, which has a simple implementation (about 120 lines of Python code), and is several orders of magnitude faster than the

previously presented technique [4] (about 87× for a typical 2D case).
- We demonstrate our multiscale decomposition on analytically designed as well as simulated turbulent flows. We show that our approach enables extraction of multiscale features, such as nested vortices. We also show that the proposed technique produces features that are stable in scale-space, and can be applied to unsteady flows by decomposing flow at each time-step independently.

2 Related Work

Turbulent flows are known to contain features on a wide (and continuous) spectrum of scales. Characterizing the inherent multiscale features of turbulence has been a long-standing problem in fluid dynamics [1], and scientists are interested in characterizing whether or not there exist universal structures across scales. Several multiscale analysis and representation approaches have been proposed; we refer the reader to Mishra *et al.* [6], [7] for a discussion of related techniques.

The intuition about multiscale features is most often formalized using signal processing techniques, where selected filters (usually low-pass) are used to study the data at a continuous spectrum of scales, also called *scale-space* [8]. Isotropic [9], [10] as well as nonisotropic [11], [12] filtering have been used to construct the scale-space, and for smoothing and denoising vector fields. Most existing techniques apply the scale-space analysis independently to each velocity component. However, linear smoothing often fails to preserve sharp flow features (see Fig. 5 published by Tong *et al.* [13]). Furthermore, the resulting flows, especially the remainder (high-frequency) component can produce distortions that seem to not correspond to any physical feature (see Fig. 5). In general, when treating each velocity component independently, it remains unclear how to physically interpret the results, e.g., the chosen filter may not preserve conformal finite-element spaces, $H(\mathrm{div})$ and/or $H(\mathrm{curl})$. Building upon smoothing techniques, Xia *et al.* [14] proposed vector-valued wavelets, but they have primarily been used to remove additive noise [15], [16], and they share some of the limitations of smoothing.

Alternatively, Tong *et al.* [13] proposed to smooth derived fields. In particular, they decompose a given flow into a pair of potential fields, smooth these potentials, and recombine the results to obtain a "simpler" flow. This approach is based upon a fundamental result in flow analysis, the *Helmholtz-Hodge decomposition* (HHD), and results in the expected effects, i.e., enhancing or suppressing small-scale structures. Nevertheless, since smoothing is still performed using a low-pass filter, and more importantly, the two fundamental constituent potentials are smoothed independently, the physical relevance of the resulting flow remains unclear (see Fig. 5). Tong *et al.*'s approach is closely related to the decomposition presented in this paper, as we also use a variant of the HHD to create a multiscale representation. However, instead of "smoothing" the given flow, our goal is to "split" the flow based on local versus non-local effects. Sections 3 and 4 will provide mathematical details and comparisons between the two approaches.

Another related approach is the proper orthogonal decomposition (POD) [17], [18], [19], which derives a reduced-order basis from instantaneous snapshots of vector fields, and has been used extensively for extracting coherent structures from turbulent flows [20], [21]. The POD is attractive due to its linearity. However, since the POD basis are derived from the global flow behavior, the resulting coarser space is comparable to the global flow decompositions. In comparison, our approach provides a way to achieve both spatial and temporal locality, and makes no assumption about the global behavior of the flow.

Decompositions of vector fields are closely related to the notion of frames of reference. In this context, the usual goal is to define a new frame of reference to facilitate analysis of flows, e.g., by extracting vortices moving along a background flow. The simplest approaches compensate for a uniform background flow [22], [23], [24], [25], [26], usually by employing the derivative of the flow. Several more general frames have also been proposed; for a complete discussion, see the survey by Pobitzer *et al.* [27]. The ideas proposed in this paper are a generalization of the internal frames of reference presented by Bhatia *et al.* [5], who used the natural HHD [4] to split a given flow into internal (local to the domain) versus external effects.

More recently, Günther *et al.* proposed rotation-invariant [28] and objective [29] detection of vortices through minimization of temporal derivatives in selected local neighborhoods. Conceptually, this approach is similar to the one presented in this paper as both techniques separate flow within a local neighborhood into different components. However, Günther *et al.*'s approach [29] aims to minimize the temporal derivative rather than considering different spatial scales, which can be a limitation since accurately estimating the temporal derivatives requires sufficiently time-resolved data, which, especially for the large simulations of greatest interest, is rarely available in practice [30]. Instead, the multiscale decomposition proposed here operates directly on individual velocity snapshots; hence, it provides many practical advantages, such as better computational cost, independence from temporal resolution, and easy applicability.

Although there exist many ways to define multiscale vector field representations, motivated by different goals and based upon different mathematical theories, only one approach (Tong *et al.* [13]) presents a multiscale decomposition, making it our primary competing approach and allowing for a direct comparison.

3 Fundamentals

This section describes the mathematical foundations required to present the discussion of our multiscale decomposition. In particular, since the Helmholtz-Hodge decomposition is defined using a set of Poisson equations, we discuss the intuition behind the Poisson equation and an important way to compute its solution before discussing the relevant decompositions.

3.1 The Poisson Equation

The *Poisson equation* is one of the most fundamental elliptic partial differential equations, and has the following form:

$$\nabla^2\phi = -f \qquad \text{in } \Omega, \tag{1}$$

where f is called the *source function*, and ϕ the *potential function*. The general solution to Equation (1) is given by a homogeneous and a heterogeneous part, written as $\phi = F + H$, where $\nabla^2 F = -f$, and H is a solution of the *Laplace equation*,

$$\nabla^2 H = 0 \qquad \text{in } \Omega,$$

and is called a *harmonic function* — a function with zero second derivative. Equation (1) is solvable only up to an additive harmonic function, and therefore, a specific H must be chosen in order to obtain a unique solution. Since a harmonic function H has a constant slope in the given domain Ω, it can be computed by using only the values at the boundary, i.e., it is determined completely by the boundary conditions.

For functions defined on infinite domains that tend to zero at infinity, there cannot exist any nonzero harmonic function. As a result, the Poisson equation can be solved uniquely without any explicit boundary conditions; however, we note the implicit assumption of a far-field boundary condition. For such cases, the fundamental solution to the Poisson equation can be computed using an integration kernel, called the *(free-space) Green's function*, $G_\infty(\mathbf{x}, \mathbf{x}_0)$, which is given as

$$\begin{aligned} G_\infty(\mathbf{x}, \mathbf{x}_0) &= -\frac{1}{2}|\mathbf{x} - \mathbf{x}_0| && \mathbf{x}, \mathbf{x}_0 \in \mathbb{R}, \\ G_\infty(\mathbf{x}, \mathbf{x}_0) &= -\frac{1}{2\pi}\log\left(|\mathbf{x} - \mathbf{x}_0|\right) && \mathbf{x}, \mathbf{x}_0 \in \mathbb{R}^2, \\ G_\infty(\mathbf{x}, \mathbf{x}_0) &= \frac{1}{4\pi|\mathbf{x} - \mathbf{x}_0|} && \mathbf{x}, \mathbf{x}_0 \in \mathbb{R}^3. \end{aligned} \tag{2}$$

The Poisson equation $\nabla^2\phi = -f$ on $\mathbb{R}^n$, where $f(\mathbf{x}) \to 0$ for $\mathbf{x} \to \infty$, can be solved by computing the *integral solution*, i.e.,

$$\phi(\mathbf{x}_0) = \int_{\mathbb{R}^n} G_\infty(\mathbf{x}, \mathbf{x}_0)\ f(\mathbf{x})\ \mathrm{d}\,\mathbf{x}. \tag{3}$$

A more detailed discussion on potential functions and integral solutions can be found in the literature [31], [32].

3.2 The Helmholtz-Hodge Decomposition

The Helmholtz-Hodge decomposition (HHD) [2], [33], [34] decomposes a given vector field into three components: a rotation-free, a divergence-free, and a harmonic vector field. Consider a smooth vector field $\vec{V} : \Omega \to \mathbb{R}^n$, where $\Omega \subseteq \mathbb{R}^n$ (for $n = 2, 3$); then

$$\vec{V} = \vec{d} + \vec{r} + \vec{h}, \tag{4}$$

where $\vec{d}$ is rotation-free ($\nabla \times \vec{d} = \vec{0}$), $\vec{r}$ is divergence-free ($\nabla \cdot \vec{r} = 0$), and $\vec{h}$ is harmonic ($\nabla \times \vec{h} = \vec{0}$ and $\nabla \cdot \vec{h} = 0$). Thus, the following equalities are obtained:

$$\begin{aligned} \nabla \cdot \vec{d} &= \nabla \cdot \vec{V}, \\ \nabla \times \vec{r} &= \nabla \times \vec{V}. \end{aligned} \tag{5}$$

To compute the decomposition, the components $\vec{d}$ and $\vec{r}$ are represented as the gradient of a scalar potential D, and the curl of a vector potential $\vec{R}$, respectively. Substituting $\vec{d} = \nabla D$ and $\vec{r} = \nabla \times \vec{R}$ in Equations (5), we get two Poisson equations,

$$\begin{aligned} \Delta D &= \nabla \cdot \vec{V}, \\ \vec{\Delta}\vec{R} &= -\nabla \times \vec{V}, \end{aligned} \tag{6}$$

where, Δ is the (scalar) Laplacian, that is, $\Delta = \nabla^2$, and $\vec{\Delta}$ is the vector Laplacian, i.e., $\vec{\Delta} = (\nabla\nabla\cdot) - (\nabla \times \nabla\times)$. The Poisson equations (6) are solved, leading to the components $\vec{d}$ and $\vec{r}$, and the harmonic component is then computed as the remainder:

$$\vec{h} = \vec{V} - \vec{d} - \vec{r}.$$

In two dimensions, the curl can be represented as a scalar value in the normal direction to the domain, leading to a simpler representation of $\vec{r}$ as the co-gradient of a scalar potential R, that is, $\vec{r} = J\nabla R$, where J is the $\pi/2$-rotation operator [35, Eq. 16]. Consequently, the second Poisson equation in (6) can be simplified as

$$\Delta R = -\nabla \cdot J\ \vec{V}. \tag{7}$$

For domains with boundaries, the solutions to the Poisson Equations (6) and (7) are not unique, and usually, boundary conditions are imposed to obtain uniqueness. Different types of boundary conditions can be applied as suited for different applications. A detailed discussion on the properties and boundary conditions of the HHD can be found in a recent survey [35].

3.3 The Natural Helmholtz-Hodge Decomposition

Recently, a new variant of the HHD, called the *natural Helmholtz-Hodge decomposition*, has been proposed that does not require specification of boundary conditions to obtain uniqueness. The natural HHD exploits the fact that the solution to the Poisson Equation (1) represents the influences that are internal (defined by f) as well as external (unknown) with respect to the given domain Ω. In this context, a harmonic function is equivalent to the external influence only, i.e., the potential generated by a source function that is zero inside Ω and (possibly) nonzero outside Ω (see [4, Section 2]).

Using this intuition, the authors proposed that the Green's function, G_∞, can also be applied to a bounded domain $\Omega \subset \mathbb{R}^n$ by splitting the computation of ϕ in Equation (3) into two parts — inside Ω and outside Ω, i.e.,

$$\phi(\mathbf{x}_0) = \int_{\Omega} G_\infty(\mathbf{x}, \mathbf{x}_0)\ f(\mathbf{x})\ \mathrm{d}\,\mathbf{x} + \int_{\mathbb{R}^n/\Omega} G_\infty(\mathbf{x}, \mathbf{x}_0)\ f(\mathbf{x})\ \mathrm{d}\,\mathbf{x}. \tag{8}$$

They noted that the second integral $\left(\int_{\mathbb{R}^n/\Omega} \cdots\right)$ creates a harmonic potential with respect to Ω, whereas the first integral $\left(\int_{\Omega} \cdots\right)$ leads to a nonharmonic potential with respect to the given domain. As a result, one way to obtain a unique solution to the Poisson Equation (1) on bounded domains is by simply discarding the second integral. Such a solution implicitly chooses to define the solution, ϕ, to be affected by internal influences only.

To compute the natural HHD, the Poisson Equations (6) are solved by splitting the solutions into two parts as in Equation (8), and then discarding the second part. Formally, the scalar and vector potentials of the natural HHD are computed as follows:

$$D(\mathbf{x}_0) = \int_\Omega G_\infty(\mathbf{x}, \mathbf{x}_0)\ \nabla \cdot \vec{V}(\mathbf{x})\ \mathrm{d}\,\mathbf{x} \qquad \mathbf{x}, \mathbf{x}_0 \in \Omega,$$
$$\vec{R}(\mathbf{x}_0) = -\int_\Omega G_\infty(\mathbf{x}, \mathbf{x}_0)\ \nabla \times \vec{V}(\mathbf{x})\ \mathrm{d}\,\mathbf{x} \qquad \mathbf{x}, \mathbf{x}_0 \in \Omega, \tag{9}$$

and the three components of the natural HHD as $\vec{d}(\mathbf{x}) = \nabla D(\mathbf{x})$, $\vec{r}(\mathbf{x}) = \nabla \times \vec{R}(\mathbf{x})$, and $\vec{h}(\mathbf{x}) = \vec{V}(\mathbf{x}) - \vec{d}(\mathbf{x}) - \vec{r}(\mathbf{x})$.

3.4 Multiscale Representation of Tong *et al.* [13]

The technique most similar to the one proposed in that proposed by Tong *et al.* [13], who extend a popular finite-element approach [36] to compute the HHD for 3D tetrahedral domains. Their approach solves a least-squares system for the Poisson Equations (6) using the boundary conditions, $\nabla D \times \vec{n} = \vec{0}$ and $\nabla \vec{R} \cdot \vec{n} = 0$, respectively. Once the two potentials (D and $\vec{R}$) have been computed, they smooth the potentials, before recombining them to create a vector field, which, in turn, is a smoother representation of the input data.

In order to provide a fair comparison with Tong *et al.*'s approach, we make two modifications to their formulation. First, their approach uses boundary conditions, which, as discussed in detail elsewhere [4], [37], can create severe artifacts not present in our approach, as our technique extends from the natural HHD. Therefore, we modify Tong *et al.*'s formulation to instead use Equation (9), thereby avoiding the otherwise present boundary artifacts. Second, since the technique as discussed by Tong *et al.* has been designed primarily for manipulating vector fields in graphics applications, not for a multiscale analysis of scientific data, their decomposition does not explicitly handle the harmonic component. In particular, the smoothed vector fields are computed by applying a low-pass filter, g_σ, on the HHD potentials: $\vec{d}_\sigma = \nabla(g_\sigma * D)$, and $\vec{r}_\sigma = \nabla \times \left(g_\sigma * \vec{R}\right)$. Here, the high-frequency component would be defined as $\vec{V} - \vec{d}_\sigma - \vec{r}_\sigma$, which expands to $\vec{h} + \vec{d} - \vec{d}_\sigma + \vec{r} - \vec{r}_\sigma$. This expression means that the harmonic component, which conceptually represents the global scale and can contain low-frequency features only, would instead be represented as part of the high-frequency flow, which is not desirable for scientific analysis. Instead, we adapt Tong *et al.*'s approach to explicitly assign $\vec{h}$ to the large-scale component.

3.5 Integral Solution in the Fourier Domain

Equation (9) represents convolution of the divergence and rotation of the field with the Green's function. The original paper on the natural HHD [4] computes the convolution spatially, i.e.,

$$\phi(\mathbf{x}) = G_\infty(\mathbf{x}) * f(\mathbf{x}), \qquad \mathbf{x} \in \Omega, \tag{10}$$

where $G_\infty(\mathbf{x}) \equiv G_\infty(\mathbf{x}, \mathbf{0})$, and $*$ is the convolution operator. Instead, we compute this convolution efficiently in the Fourier domain, although this computational gain costs some accuracy at the boundary. Since spatial convolution is effectively a weighted sum for discrete data, the boundary poses few problems as the "missing samples", i.e., the data outside the boundary, are simply taken to be zero. However, the Fourier transform is defined only for a periodic signal, and therefore, computing the transform of nonperiodic data imposes additional high frequencies on the spectrum. We also note that using windowing approaches, e.g., Hamming or Tukey window, to make the data periodic is ill-suited for vector fields because they create significantly worse artifacts due to sharp gradients near the boundary. Although vector fields of interest are almost always nonperiodic, in practice, we found that the boundary artifacts due to a nonperiodic Fourier transform are negligible for the large-scale flows of practical interest. Furthermore, considering the computational advantage of convolution in the Fourier domain ($\mathcal{O}(n \log n)$) over that in the spatial domain ($\mathcal{O}(n^3)$ in 3D), such artifacts are acceptable.

4 Multiscale Decomposition

This paper presents a new *multiscale* kernel to solve the Poisson equation. We use the presented multiscale solution to the Poisson equation to decompose vector fields using the *multiscale Helmholtz-Hodge decomposition*. The defining characteristic of this decomposition is that given a scale, the flow is decomposed into two components, which contain features with respect to the corresponding scale (akin to low- and high-frequency components in filtering). In particular, the goal is to define a *small-scale flow* containing small-scale features (local with respect to the given scale), with the difference containing the remaining large-scale (nonlocal) structures.

Tong *et al.* compute two potential fields, D and $\vec{R}$, and smooth them using a low-pass filter. They show that, using the HHD, their approach can better preserve sharp features in the flow, compared to direct linear smoothing of the vector field. Nevertheless, the artifacts of smoothing can still be observed, e.g., the approach is not able to distinctly decompose the flow into local versus nonlocal features, e.g., see Fig. 5. We note that the smoothed potential field, D_σ, used by Tong et al.'s approach is given as

$$\begin{aligned} D_\sigma &= g_\sigma * \left(G_\infty * \nabla \cdot \vec{V}\right), \\ &= (g_\sigma * G_\infty) * \nabla \cdot \vec{V}. \end{aligned}$$

Thus, this approach is equivalent to solving the Poisson Equation (6) using the integral solution (11), but using a smoothed Green's function as the integration kernel.

4.1 Multiscale Solution to the Poisson Equation

In order to explore the limitations of smoothing approaches, and to develop a new multiscale decomposition of vector fields based on the idea of *"splitting"* local versus nonlocal effects, we propose a new *multiscale filter* to solve the Poisson equation. This section discusses the properties and implications of the effective integration kernel of Tong *et al.*' s approach, as well as our proposed kernel.

Given a Poisson equation, the goal is to find the potential function with respect to a given scale, σ. Traditionally, the focus has been on the smoother function containing only the large-scale components, but in many cases, the small-scale, local components are as important.

Smoothing Approaches. There are two common strategies to obtain the low-frequency component. As suggested by Tong *et al.*, one can smooth the potential function after solving the Poisson equation using the integral solution given

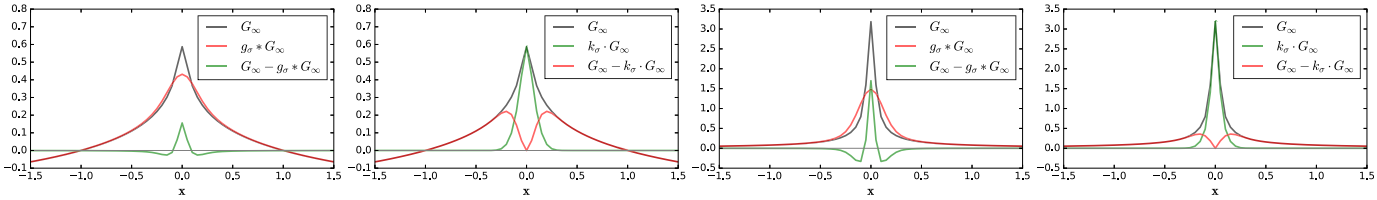

(a) 2D smoothing filters (b) 2D modified Green's functions (c) 3D smoothing filters (d) 3D modified Green's functions

Fig. 2. Comparison of filters for computing the multiscale Poisson equation in 2D (a,b) and 3D (c,d). The effective filters for smoothing are shown in (a) and (c) and those corresponding to the proposed Green's function in (b) and (d). The red and green curves show filters for extracting large- and small-scale components, respectively. As seen from the figure, the modified Green's function maintains the weights in the local neighborhood (of $\mathbf{x} = \mathbf{0}$) better, and thus, provides a "splitting" of local versus nonlocal influences compared to "smoothing" filters. We use a normalized Gaussian ($g_\sigma(\mathbf{0}) = 1$) as the scaling function k_σ for all results in the paper.

by Equation (3), i.e., $\phi_\sigma = g_\sigma * \phi = g_\sigma * (G_\infty * f)$, where g_σ is a low-pass filter, e.g., a Gaussian filter. Alternately, one can first simplify the source function leading to a simplified potential, i.e., $\phi_\sigma = G_\infty * (g_\sigma * f)$. Since convolution is associative, both these approaches are mathematically equivalent to smoothing the Green's function and then solving the Poisson equation, i.e.,

$$\phi_\sigma = (g_\sigma * G_\infty) * f. \tag{11}$$

Using the distributive property of convolution, the implied kernel for the small-scale component, ψ_σ, can be derived as follows:

$$\begin{aligned} \psi_\sigma &= \phi - \phi_\sigma \\ &= G_\infty * f - (g_\sigma * G_\infty) * f \\ &= (G_\infty - g_\sigma * G_\infty) * f. \end{aligned} \tag{12}$$

Figs. 2a and 2c show the implied kernels for both small- and large-scale components in the standard smoothing approaches. As expected, the low-pass filter (red) smoothes out the singularity at $\mathbf{x} = \mathbf{0}$, suppressing the convolution weights in the immediate neighborhood. The high-pass filter (green) captures the remaining weights. Although mathematically valid, smoothing does not produce the desired result in the physical sense of the Poisson equation, because despite suppressing certain frequencies while retaining others, it fails to maintain the spatial context of the Poisson equation. Note how the local influences (at and near $\mathbf{x} = \mathbf{0}$) are distributed between the two scales, and thus do not provide a clean separation into local versus nonlocal effects.

The Modified Green's Function. Recall that the integral solution (3) determines the potential ϕ at a given point by accumulating the net influence of the source function f at all the points in the domain. Thus, a *spatially relevant* solution at a reduced scale can be obtained by explicitly controlling the weights in the (spatial) neighborhood of the given point. Figs. 2b and 2d show our proposed kernel, whose mathematical properties are discussed in the next paragraph. In particular, note that the filter for small-scale features (green) preserves not only the singularity, but also the weights in the immediate neighborhood, thus capturing local influences with higher fidelity. As a result, the corresponding filter for large-scale effects (red) does not include the point $\mathbf{x} = \mathbf{0}$ and suppresses the contribution of neighboring points. Furthermore, the large-scale filter preserves the weights in the far-field. Such a kernel can be thought of as a *modified Green's function*, and is better suited to compute multiscale solution to the Poisson equation.

Mathematically, the modified Green's function can be obtained by multiplying it by the Green's function with a suitable scaling kernel, $k_\sigma(\mathbf{x}) : \mathbb{R}^n \to \mathbb{R}$, with the following restrictions:

- For any given scale σ,
  - $k_\sigma(\mathbf{x}) = 1$ for $\mathbf{x} = \mathbf{0}$,
  - $k_\sigma(\mathbf{x}) \to 0$ for $\mathbf{x} \to \infty$,
  - $0 \leq k_\sigma(\mathbf{x}) \leq 1$ for all $\mathbf{x}$, and
  - $k_\sigma(\mathbf{x}_1) \geq k_\sigma(\mathbf{x}_2)$ for all $|\mathbf{x}_1| \leq |\mathbf{x}_2|$.
- For any two scales $\sigma_1 < \sigma_2$,
  - $k_{\sigma_1}(\mathbf{x}) \leq k_{\sigma_2}(\mathbf{x})$ for all $\mathbf{x}$.

Two simple choices for k_σ are a normalized Gaussian function and a tent function, where the spread of the function is proportional to σ. For $k_\sigma = 1$, the Green's function remains unchanged, and therefore, a full-scale solution is obtained.

The crucial difference with the smoothing approach is that when using the modified Green's function, compared to Equation (12), we directly compute the small-scale potential, ψ^*_σ, as the integral solution to

$$\psi^*_\sigma = (k_\sigma \cdot G_\infty) * f. \tag{13}$$

Smoothing versus Splitting. Conceptually, the modified Green's function is a high-pass filter, compared to the low-pass filter given in Equation (11). However, since the proposed modification (k_σ) explicitly constricts the Green's function in the spatial domain, our proposed filter is better suited for "splitting" the local effects from nonlocal ones, compared to the "smoothing" performed by low-pass filters. Next, we will demonstrate the advantages of the modified Green's function in the context of vector fields.

4.2 The Proposed Multiscale Decomposition

Using the multiscale solution to the Poisson equation, computation of the multiscale HHD is straightforward. In particular, the two small-scale potentials, denoted $\hat{D}^*$ and $\hat{\vec{R}}^*$, respectively, can be computed as

$$\begin{aligned} \hat{D}^*_\sigma &= (k_\sigma \cdot G_\infty) * \nabla \cdot \vec{V}, \\ \hat{\vec{R}}^*_\sigma &= (k_\sigma \cdot G_\infty) * \nabla \times \vec{V}, \end{aligned} \tag{14}$$

giving the small-scale flow component, $\vec{l}^*_\sigma$ as

$$\vec{l}^*_\sigma = \hat{\vec{d}}^*_\sigma + \hat{\vec{r}}^*_\sigma = \nabla \hat{D}^*_\sigma + \nabla \times \hat{\vec{R}}^*_\sigma,$$

and the large-scale component as $\vec{h}^*_\sigma = \vec{V} - \vec{l}^*_\sigma$.

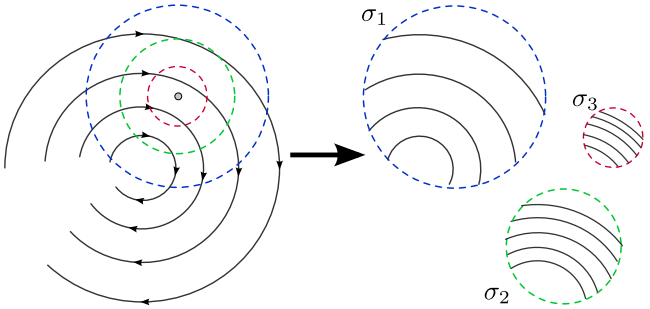

Fig. 3. Considering neighborhoods of varying sizes allows creating a multiscale decomposition by representing different amounts of rotation (and divergence) as nonlocal effects. Aggregating only the local effects, thus, amounts to creating a small-scale flow, i.e., containing only the features at or below the given scale. For example, as the smallest neighborhood (red) sees a mostly laminar flow, the corresponding small-scale features have little rotation, and the large-scale rotation can be used to effectively create a rotational frame of reference.

The intuition behind the multiscale HHD is schematically illustrated using Fig. 3. Without loss of generality, consider a rotational vector field in 2D, and the solution of Equations (14) for a single point, $\mathbf{x}_0$ (shown as a gray dot) for three scales, $\sigma_1 > \sigma_2 > \sigma_3$. The corresponding scaling functions gradually and smoothly scale the Green's function down to zero for the neighboring points in an isotropic manner. The blue, green, and red circles in the figure show the distances from $\mathbf{x}_0$ (the gray dot), where $k_\sigma \cdot G_\infty$ becomes negligible for three scales, respectively.

Zooming into the three circles separately, the figure shows *only* the flow considered by Equations (14) for $\mathbf{x}_0$ for the different scales. The solution to these equations considers the divergence and rotation *only* in the corresponding region, and "approximates" a vector at $\mathbf{x}_0$ that best describes the divergence/rotation within the domain, thus capturing the phenomena that are *local with respect to the given scale*. These ideas generalize to compressible flows where the local phenomena capture both compressibility and rotation. Furthermore, following the discussion in Section 3.3, any divergence/rotation at the points outside these boundaries creates a harmonic flow with respect to the corresponding region. When combined globally, the sliding window implied by the convolution operator allows removing the larger-scale rotation with respect to the smaller regions in the domain.

When the entire given domain is considered, this approach is equivalent to creating the (globally) harmonic flow [5]. On the other hand, with decreasing scale, the given rotational field disappears from the small-scale component, and contributes to the large-scale part. For the smallest scale in this experiment, the rotational component is zero, whereas the large-scale component is no longer harmonic and contains all of the rotational field. Indeed, in the limiting case of an infinitely small neighborhood, the multiscale decomposition creates a Lagrangian viewpoint, where the entire motion is seen relative to a given observer, who is considered to be at rest.

4.3 Multiscale Decomposition of Unsteady Flows

The description of our multiscale decomposition framework depends only on the spatial derivatives (on the divergence and curl) local to a spatial neighborhood. Indeed, the independence from the temporal dimension is a key characteristic of our framework. Given a temporally smooth unsteady flow, the decomposition can be applied to each time-step individually to produce a temporally smooth unsteady decomposition that captures the multiscale behavior of interest.

5 Results

We demonstrate our multiscale decomposition on simulated flows, a jet in crossflow and a lifted ethylene flame, both of which are expected to contain nested vortices across scales.

5.1 Jet in Crossflow

Our first test case is a common type of turbulent flow: a jet in crossflow [38], which is a fundamental flow phenomenon relevant to many engineering applications, e.g., film cooling of turbines, fuel injections, and dilution jets in gas-turbine

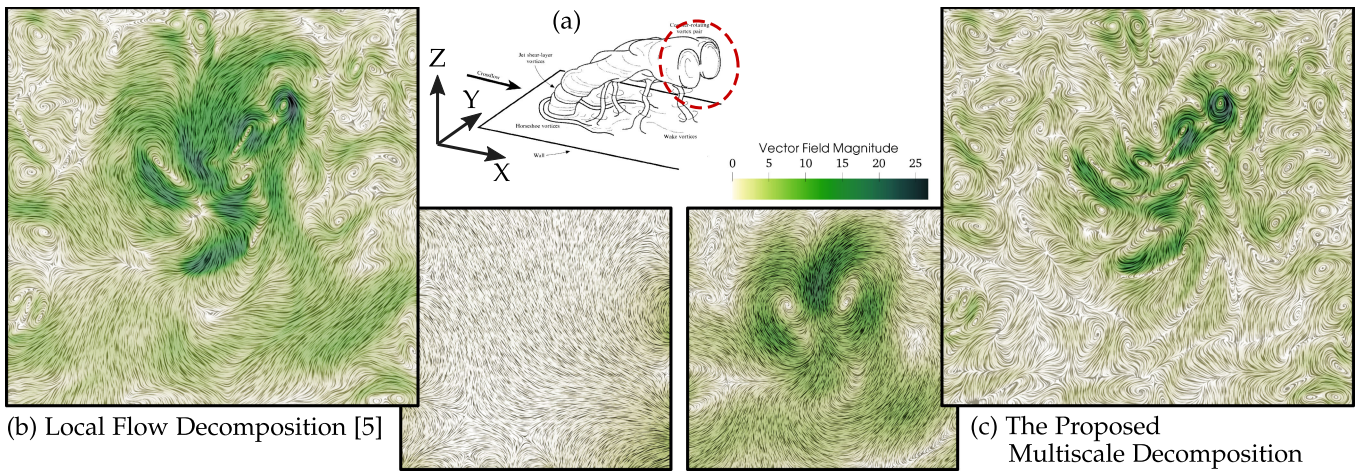

Fig. 4. (a) Illustration of a jet in crossflow and the different types of vortical structures associated with this flow; the most important, and yet the most elusive to find, is the counter-rotating vortex pair, which represents weak, large-scale rotation, typically not detectable using standard approaches in the original flow (not shown) or existing decomposition techniques. (b) The local flow (as defined by Bhatia *et al.* [5]) on the slice as a LIC image and the corresponding global flow as streamlines. The expected vortices are too small to influence the global flow but are also not easily recognized in the superposition of all nonglobal effects (LIC). (c) The proposed multiscale decomposition at an appropriate scale, which highlights the vortex pair in the large-scale component (streamlines) and well-defined nested vortices in the small-scale component (LIC).

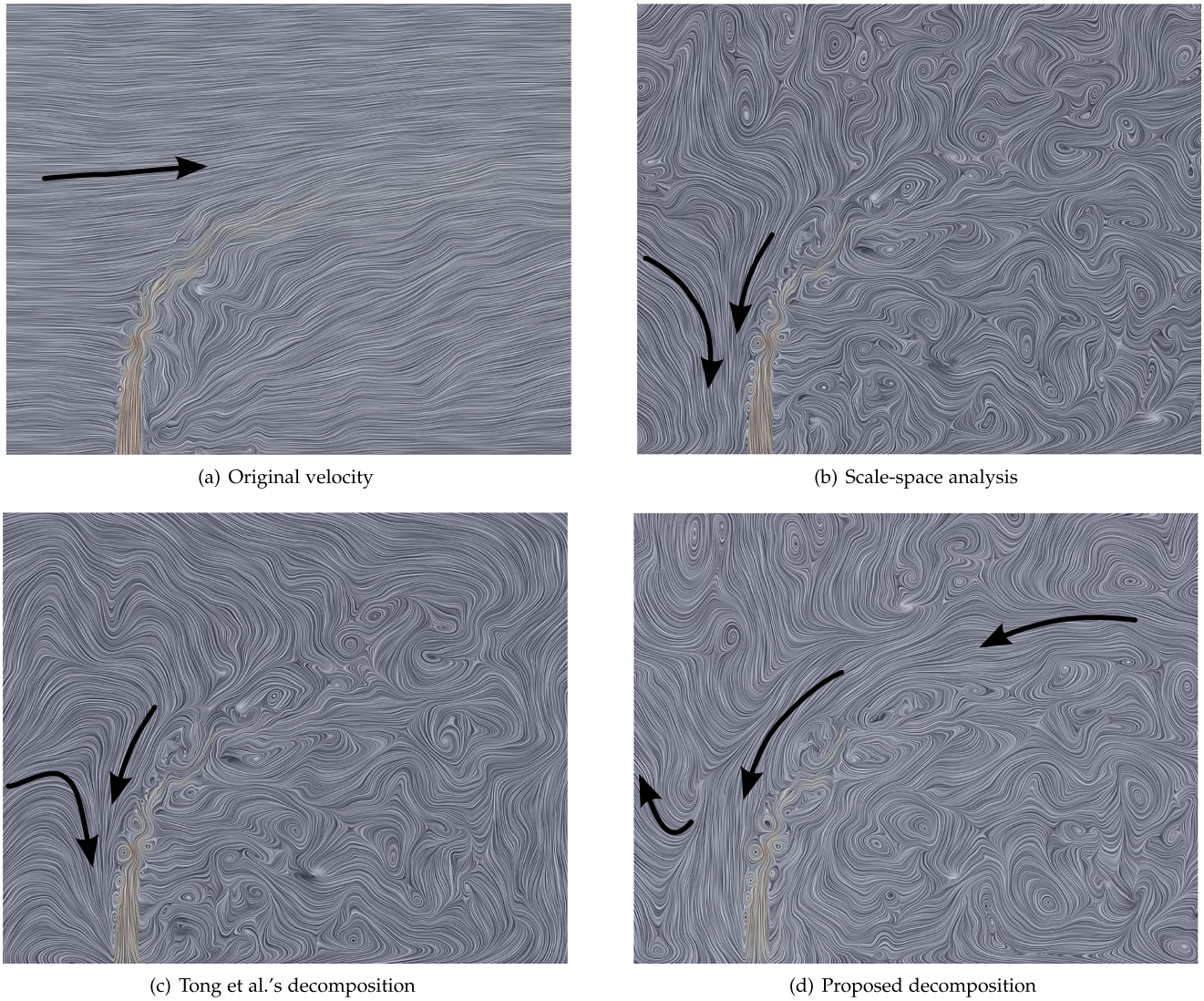

(a) Original velocity (b) Scale-space analysis

(c) Tong et al.'s decomposition (d) Proposed decomposition

Fig. 5. Multiscale analysis of a jet in crossflow. (a) The original velocity field at the center of the jet, within the lateral direction (xz-plane); (b) the high-frequency component of a traditional scale-space analysis showing a number of unphysically distorted regions; (c) the high-frequency component using Tong *et al.*'s multiscale decomposition [13] shows fewer artifacts but still fails to resolve the flame; and (d) the small-scale flow computed by the proposed technique resolves the expected behavior on top of the flame. In this comparison, only the proposed decomposition correctly identifies the reverse flow above the jet, indicating the drag induced by the turbulent flame on the crossflow.

combustors. The experimental set-up contains an injection of flow through a jet at the bottom in the presence of a strong background flow in the transverse direction, the crossflow, as illustrated in Fig. 4a. The goal of the experiment is to study different types of vortical structures created by the interaction of the burning jet with the crossflow.

Important structures in this flow include a pair of counter-rotating vortices, which occur as a result of the impulse of the jet on the crossflow, and become dominant in the far field. Experts speculate that various smaller vortices are nested inside these larger counter-rotating vortices. However, due to the turbulent nature of the phenomenon, these large, but weak, vortices are overpowered by the smaller and stronger vortices, making them difficult to extract using standard approaches. Previously, by compensating for the global harmonic background flow, Bhatia *et al.* [5, Fig. 11] used internal reference frames to extract and highlight these features of interest.

Using Fig. 4, we show that our proposed technique improves upon their approach by enabling the extraction of these vortices through a multiscale decomposition of the flow directly on a relevant 2D slice (in xy plane). In particular, Fig. 4a shows the existing decomposition [5], which shows turbulent behavior in the local component, and that the global component is a harmonic flow with very low magnitude. Such behavior is observed due to a lack of separation of scale of vortices. The results of the proposed multiscale decomposition for a selected scale are shown in Fig. 4c. As seen in the figure, the nonlocal component captures the counter-rotating vortices, thus creating a rotational frame of reference for the smaller, nested vortices, which can be found in the local component. Advancing the state of the art from the global decomposition, this result allows domain experts to simultaneously analyze both types of vortices (nested as well as counter-rotating) to understand the effects of simulation parameters. We note that the

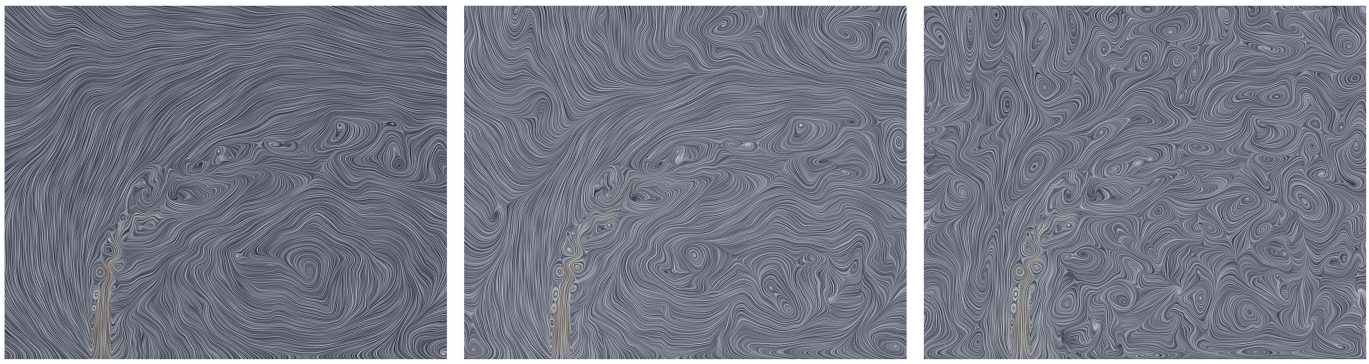

Fig. 6. Multiscale decomposition of the flow shown in Fig. 5a defined on a 20×25 mm domain at decreasing scales ($\sigma = 6.67, 3.70, 1.48$ mm) from left to right. One interesting structure is the single dominant vortex under the jet arch highlighted at the largest scale. Subsequent scales show successively smaller vortices, confirming the intuition of nested vortical structures.

projection step to compute the xy slice for this experiment discards the crossflow, which is orthogonal to the chosen slice, since the experiment focuses largely on the counter-rotating vortex pair.

We next analyze the data in an orthogonal direction, on a xz slice through the center of the jet (see Fig. 5). In this case, the goal is to study the features around the flame, and therefore, the projection discards the y component of the flow, which although not zero, is negligible compared to the strong crossflow. The given flow, as shown in Fig. 5a, highlights the jet emerging from the bottom of the domain, as well as the strong crossflow in the lateral direction. Fig. 5d shows the small-scale flow obtained through our approach. At the chosen scale, the resulting flow captures not only the jet, which contains a series of small but strong jet shear-layer vortices, but also a number of other turbulent structures in the domain. Although many similar structures are observed when Gaussian filtering (Fig. 5b) and Tong *et al.*'s approach (Fig. 5c) are applied for the same σ, what distinguishes the three results is the shape and direction of the flow above the jet flame as it moves to the right. Our decomposition highlights the expected (mostly laminar) flow around the flame. Note that in the small-scale component, i.e., relative to the strong crossflow, the flow direction is inverted, indicating the drag the flame induces on the surrounding flow. The other approaches resolve the same features in the simple, nonturbulent flow directly at the front of the flame, but fail to do so in the more complex environment at the back of the flame.

Next, in Fig. 6, we present the multiscale decomposition on the same xy slice for progressively smaller σ, thus focusing on increasingly smaller vortices. The figure shows the expected correspondence between the size of our integration kernel and the size of the vortices observed. Results like this can be used to explore the distribution of features, e.g., vortices at different scales, and the resulting energy cascading effects with respect to scale. The scale-space of features is further discussed in Section 5.3.

Finally, the multiscale HHD can be used directly on the 3D flows as well. Fig. 7 presents the decomposition for two different scales; the figure shows the magnitude of vorticity, as well as the LIC visualization of a slice (computed after performing the 3D decomposition). As can be seen from the figure, the proposed multiscale decomposition highlights smaller scale features in the flow. It is important to note that the HHD (and hence the proposed multiscale approach) does not commute with the 2D projection (slicing) operator; therefore, unsurprisingly, the LIC visualizations in Fig. 7 show different flows than those in Fig. 6.

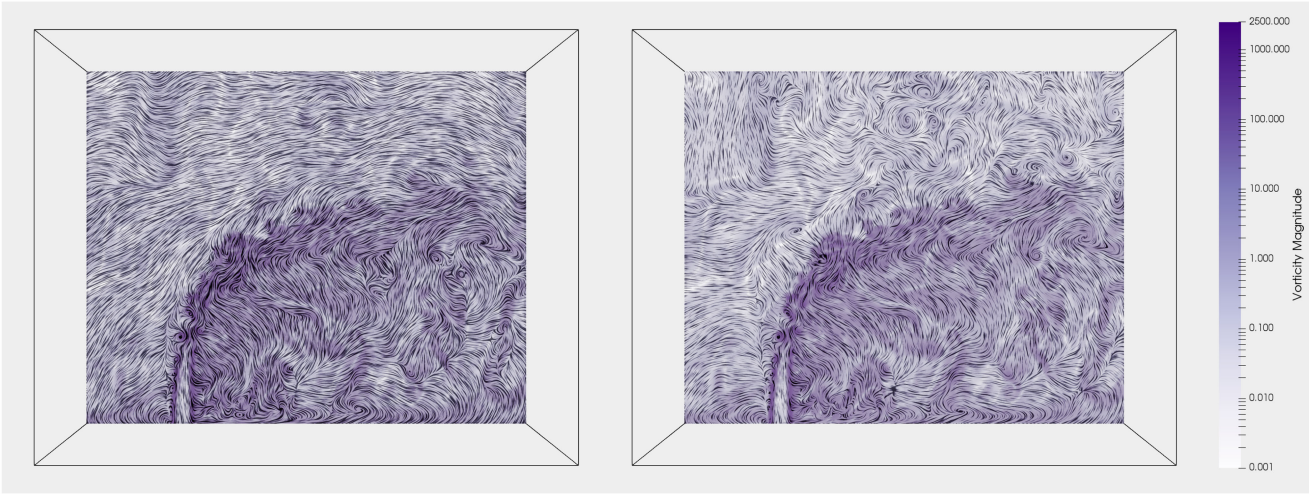

Fig. 7. Local (high-frequency) components of the JICF computed using the proposed decomposition at full scale (left) and a smaller scale (right, $\sigma = 0.925$ mm) show substantial differences, with the latter focusing more on finer features. The images show the vorticity (log-mapped to the shown color scale) superposed on the LIC visualization of the flow through the center of the flame, highlighting the difference in flow structures.

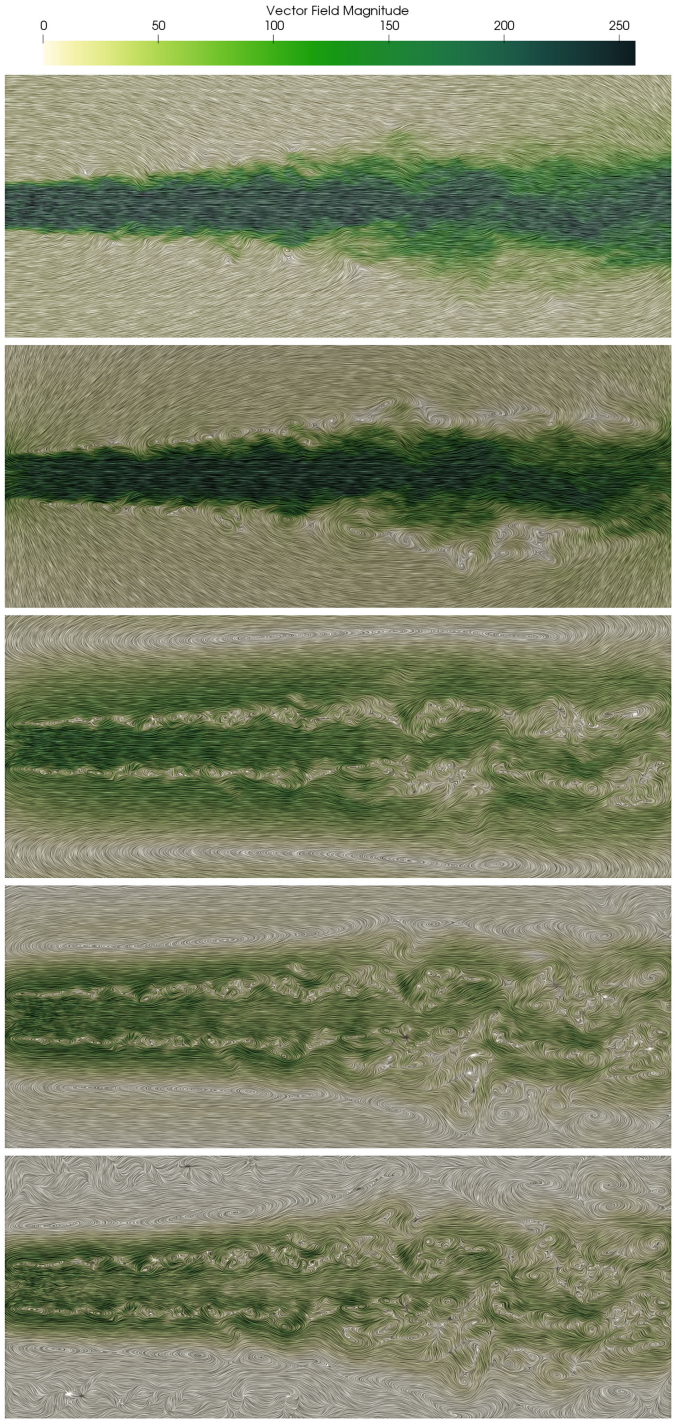

Fig. 8. Velocity field of a lifted ethylene jet flame (top) in a domain size of 20.25×8.0 units is decomposed into its local component at the global scale (second from top), which highlights a strong through flow, but fails to resolve nesting of vortices. The next three images show the multiscale decomposition for decreasing scales, $\sigma = 2.0$, 1.0, 0.6 units, respectively, which demonstrate increasingly smaller vortices, nested inside prominent counter-rotating vortices.

5.2 Lifted Ethylene Jet Flame

Next, we analyze a direct numerical simulation of a turbulent lifted ethylene jet flame [39], which represents a compressible and highly turbulent flow. In this case, fuel is injected from the left of the domain, creating a strong background flow toward the right. This type of flow is well studied, and is known to contain nested turbulent structures. Therefore, this data provides important validation for our approach. Fig. 8 shows the given flow as well as the local components of our multiscale decomposition for a variety of scale parameters. At the full scale, the local component is heavily influenced by the divergence created by the jet. At the next scale shown, however, almost all the divergence has been removed from the local component, and the resulting flow shows nested vortical structures. In particular, with decreasing scale, increasingly smaller rotational features are observed.

5.3 Stability of the Multiscale Decomposition

Scientific data, like the ones discussed above, rarely provides a "ground truth" against which validity of a new technique may be established. However, it is known that physically relevant features must be stable with respect to the multiscale decomposition [10], [40]. Therefore, we demonstrate the stability of the features identified through the proposed decomposition.

We revisit the xz and yz slices of the jet in crossflow discussed earlier, and compute the decomposition for a wide range of scales. We compute the critical points of the resulting fields in a numerically robust manner [41] and track them over scales, i.e., compute mapping of critical points within adjacent scales using spatial distance. As shown in Fig. 9a, the "scale-space" of critical points computed in the manner described above shows long and stable paths of critical points, suggesting that several features remain persistent over the considered range of scales, although some are indeed short-lived, and limited in scale. In particular, many of the strong vortices in the (xz-σ domain; left of Fig. 9a) span a wide range of scales. Furthermore, the result for the yz-σ scale-space shows a larger number of shorter tracks, indicating that many identified features are limited in scale. A closer examination shows the equivalent of Hopf-bifurcations in scale space with pairs of counter-rotating vortices appearing at smaller scales. Despite the seemingly noisy figure, the merging of many of the tracks can be noticed (especially in the yz-σ scale-space). These features represent smooth and stable merging of features, confirming that the decomposition does not create artifacts in the form of suddenly appearing critical points (except at the boundary of the domain). The xz slices also contain some prominent vortices that are long-lived yet shift their position significantly throughout the scales. This phenomenon is well known in scale-space analysis, and indicates that these structures are relevant (and stable) for some but not all scales.

5.4 Multiscale Decomposition of Unsteady Flows

To demonstrate the decomposition of unsteady flows, we create a steady flow with four rotating centers [28] and add to it a time-varying unsteady vortex. The resulting flow represents a key test case where the flow behavior of a larger vortex may overwhelm that of smaller vortices. For example, in our test scenario, even though the four centers are stationary, the pathlines, which are also affected by the unsteady rotation, fail to swirl around and capture the stationary (and known) centers of rotation (Fig. 1a).

Fig. 1 also visualizes the small-scale and large-scale components with respect to a chosen scale. The small-scale flow

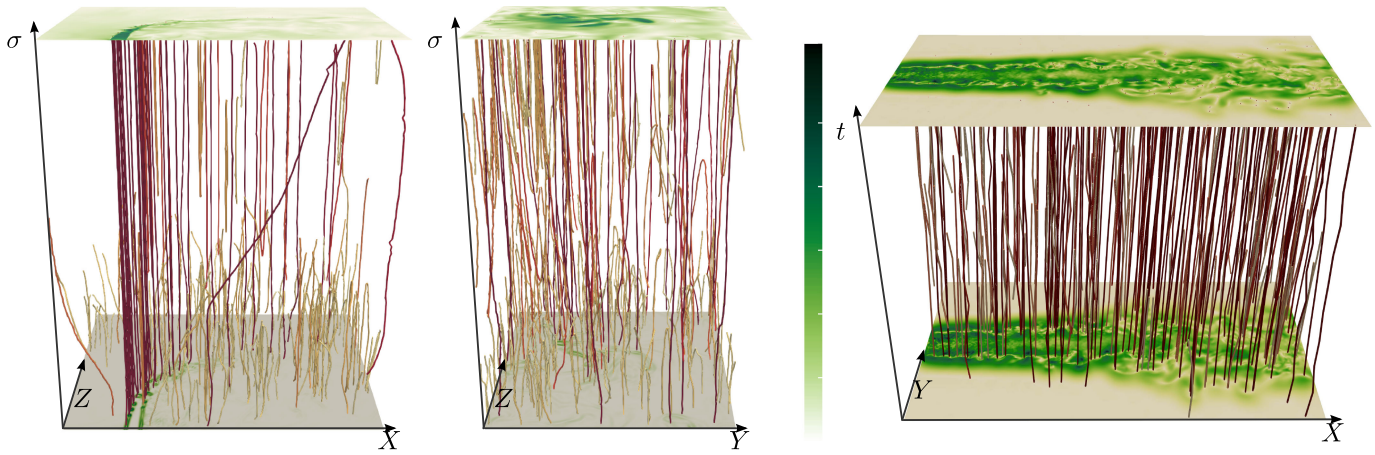

(a) Scale-space for two 2D planes of the jet in crossflow. (b) Time-varying lifted ethylene jet flame.

Fig. 9. Stability of the proposed decomposition can be demonstrated by studying features of the components across scale and/or time. (a) The paths of critical points in the "scale-space" for two orthogonal slices of the jet in crossflow for $\sigma \in [0.0925, 9.8975]$. (b) The paths of critical points across time for the lifted flame show. All paths are colored yellow–red with increasing persistence (approximated as the length of the paths). Long stable curves and smooth merging of curves demonstrate that the proposed decomposition produces stable features, with respect to both scale and time. The bounding slices are visualized with the magnitude of the local flow mapped to the color scale ([0,303] for (a) and [0, 257] for (b)).

in this case is able to completely capture the stationary centers of rotation, as seen both by the LIC visualization as well as the swirling pathlines around the centers. In contrast, the large-scale flow captures the time-dependent rotation in the flow, and highlights its larger spatial span (scale).

Next, Fig. 9b visualizes critical point tracking for the time-varying lifted flame for a single scale. As can be noticed from the figure, most critical points persist over the entire time span and show stable paths, indicating temporal stability in the results computed using individual time-steps. This result is different from Fig. 1 in two ways. First, we show the temporal stability of critical points as compared to pathlines swirling around known vortices in Fig. 1. Second, whereas the centers of rotation in Fig. 1 were stationary, the critical points in the lifted flame are unsteady. Our experiments illustrate a temporally smooth, multiscale decomposition of unsteady flows, which is able to extract the evolution of multiscale features by decomposing individual time-steps of unsteady flows.

5.5 Implementation and Performance

The computation of the natural HHD as described by Bhatia *et al.* [4], and further improved upon by us (see Section 3.5), requires (1) gradient, divergence, and curl operators; (2) a convolution operator; and (3) the computation of the Green's function, G_∞. The proposed multiscale decomposition additionally requires (4) the computation of the scaling kernel, k_σ, and (5) the multiplication of k_σ with G_∞. It is important to note that since steps 4 and 5 always perform a single multiplication (per grid point) irrespective of the chosen scale, the computational cost is independent of σ. We have prototyped this pipeline in Python, leveraging the inbuilt functionalities provided by `numpy` and `scipy`, thereby allowing the implementation of the entire approach in about 120 lines of code.

The time to compute the decomposition for a flow defined on $[1408 \times 1080]$ slice is $\approx$3.3 seconds on a standard laptop computer. The 3D computation is more intensive, as convolution steps take $\approx$347 seconds each for a $[352 \times 275 \times 270]$ dataset, making the time needed for four convolutions $\approx 92\%$ of the total time. Since the primary computational bottleneck is solving 3D convolutions, we are exploring the `fftw` library [42], which is likely to be more optimized than `scipy`'s implementation. Nevertheless, our approach provides a computational gain of several orders of magnitude over the previous work [4], which reported requiring $\approx$290 seconds for a 2D decomposition on a $[800 \times 2025]$ grid using 144 processes for spatial convolution.

6 Conclusion

We present a new perspective on creating multiscale representations for vector fields. Unlike conventional scale-space approaches, which operate primarily in the frequency domain and perform *smoothing* of the given data, our technique is motivated by the physical intuition of *splitting* the flow into components corresponding to spatial scales. We present a new multiscale kernel for Poisson equation to support splitting operations. We show that the proposed approach allows separating phenomena existing at different scales, and extracting features that are stable and physically meaningful. Since it is based on convolutions, the proposed approach is robust against noise. Several of our results show features that are expected, but have not been directly observed previously. Furthermore, the features generated by the proposed decomposition are stable in the scale-space, which is well known [10], [40] to be a strong indicator of physical relevance of features. As a result, we argue that our technique is well suited for simultaneous visualization and analysis of flow features at different scales.

Our approach is based on potential theory, which provides a mathematical framework to represent the underlying Poisson equations at multiple scales using the proposed *modified Green's function*. The discussion presented in this paper is valid for 1D, 2D, and 3D vector as well as scalar functions, although the current work has been motivated by the need to represent multiscale flow features. We would like to investigate the applications of the multiscale Poisson equation for scalar functions as well.

This paper describes a framework to decompose a flow with respect to scales; however, a current limitation is the lack of understanding of how to choose an appropriate scale. We are currently exploring this question and plan to consider transfer of energy across scales to find distinguished scales that are meaningful for analysis.

We note that the multiscale effects in 3D appear muted when compared to the 2D results, i.e., the flow features vary less across scales. One explanation is that the 3D Green's function is much narrower than its 2D equivalent, as shown in Fig. 2. As a result, even at the full scale (i.e., [5]), the 3D results are already very localized, and therefore, further restricting the kernel has less of an impact. As part of future work, we would like to better understand this effect and explore new scaling functions for 3D. For example, one might artifically inflate the 3D Greens's function, and thus extract features at scales larger than what we now consider "global", although it is unclear how this would connect to the mathematical theory. Alternatively, one might find that a 3D harmonic flow can simply represent a much richer set of structures than a 2D harmonic. Such a finding would explain how the global background flow in 3D is able to express much of the complexity, leaving few structures for the local component. In this case, one might consider adding additional constraints on the background flow, e.g., by restricting it to lower frequencies, i.e., smoother flows.

Although defined using a spatial kernel, our approach is directly applicable to computing multiscale decomposition of unsteady flows by decomposing individual snapshots. Our results demonstrate that not only does the presented method preserve the temporal stability of data, but is also able to extract stationary or nonstationary features with respect to scales. Decoupling the temporal dimension from the analysis offers significant advantages for large-scale data, where limited I/O bandwidth makes the availability of data at sufficient temporal resolution prohibitive [30]. As compared to the techniques that compute temporal derivatives, which makes them susceptible to errors at insufficient resolution, our approach is agnostic to the temporal sampling rate, and produces temporally smooth decompositions given temporally smooth flows, thus alleviating the dependence on high temporal resolution. Additionally, processing time-steps of unsteady flows independently makes the approach embarrassingly parallel.

One intriguing interpretation of the multiscale decomposition is to consider the results in the context of new frames of reference, i.e., as a multiscale extension of the internal reference frames [5]. Traditionally, flow fields have been considered primarily in two frames of reference: the Eulerian frame, used by most simulations, and the Lagrangian frame, moving along each particle. The internal frame [5] (and related ideas, such as the local flow [43]) adds an intermediate frame that roughly corresponds to a single global observer moving with a background flow. Conceptually, the multiscale decomposition proposed here adds a continuous scale of observers corresponding to different spatial scales, which can be seen as a continuous set of frames that cover the entire range from the Lagrangian viewpoint (infinitely small scales) to the Eulerian viewpoint (infinitely large scales) and anywhere in between. Our results show a number of expected features in well-known flows and demonstrate that intermediate scales do extract physically meaningful features. However, going forward, it will be crucial to develop both theory and algorithms to determine which scales are most important for any given flow and how to connect the results to the intuition on local flow behavior.

Acknowledgments

This work was performed under the auspices of the U.S. Department of Energy (DOE) by Lawrence Livermore National Laboratory (LLNL) under contract DE-AC52-07NA27344. The second author acknowledge support from ARO W911NF-15-1-0222 (Program Manager Dr. Mike Coyle). This work was supported in part by the DOE, National Nuclear Security Administration (NNSA), under Award Number(s) DE-NA0002375. This research was supported in part by the Exascale Computing Project (17-SC-20-SC), a collaborative effort of the DOE Office of Science and the NNSA. NSF OAC award 1842042. NSF OAC award 1941085. NSF CMMI award 1629660. LLNL Release: LLNL-JRNL-743978.

References

[1] P. Sagaut, S. Deck, and M. Terracol, *Multiscale and Multiresolution Approaches in Turbulence*. Singapore: World Scientific Pub. Comp., 2013.

[2] H. Helmholtz, "Über Integrale der hydrodynamischen Gleichungen, welche den Wirbelbewegungen entsprechen," *J. für die reine und Angewandte Mathematik*, vol. 1858, no. 55, pp. 25–55, Jan 1858.

[3] H. Lamb, *Hydrodynamics*, 6th ed. Cambridge, U.K.: Cambridge Univ. Press, 1932.

[4] H. Bhatia, V. Pascucci, and P.-T. Bremer, "The natural Helmholtz-Hodge decomposition for open-boundary flow analysis," *IEEE Trans. Vis. Comput. Graph.*, vol. 20, no. 11, pp. 1566–1578, Nov. 2015.

[5] H. Bhatia, V. Pascucci, R. M. Kirby, and P.-T. Bremer, "Extracting features from time-dependent vector fields using internal reference frames," *Comput. Graph. Forum*, vol. 33, no. 3, pp. 21–39, Jun. 2014.

[6] M. Mishra, X. Liu, M. Skote, and C.-W. Fu, "Kolmogorov spectrum consistent optimization for multi-scale flow decomposition," *Phys. Fluids*, vol. 26, no. 5, 2014, Art. no. 055106.

[7] X. Liu, M. Mishra, M. Skote, and C.-W. Fu, "On visualizing continuous turbulence scales," *Comput. Graph. Forum*, vol. 38, no. 1, pp. 300–315, 2019.

[8] T. Lindeberg, "Scale-space theory: A basic tool for analysing structures at different scales," *J. Appl. Statist.*, vol. 21, pp. 224–270, 1994.

[9] D. Bauer and R. Peikert, "Vortex tracking in scale-space," in *Proc. Symp. Data Vis.*, 2002, pp. 233–ff.

[10] T. Klein and T. Ertl, "Scale-space tracking of critical points in 3D vector fields," in *Topology-based Methods in Visualization*, H. Hauser, H. Hagen, and H. Theisel, Eds. Berlin, Germany: Springer, 2007, pp. 35–49.

[11] T. Preußer and M. Rumpf, "Anisotropic nonlinear diffusion in flow visualization," in *Proc. Conf. Vis.*, 1999, pp. 325–332.

[12] U. Diewald, T. Preußer, and M. Rumpf, "Anisotropic diffusion in vector field visualization on euclidean domains and surfaces," *IEEE Trans. Vis. Comput. Graph.*, vol. 6, no. 2, pp. 139–149, Jun. 2000.

[13] Y. Tong, S. Lombeyda, A. Hirani, and M. Desbrun, "Discrete multiscale vector field decomposition," *ACM Trans. Graph.*, vol. 22, no. 3, pp. 445–452, 2003.

[14] X.-G. Xia and B. W. Suter, "Vector-valued wavelets and vector filter banks," *IEEE Trans. Signal Proc.*, vol. 44, no. 3, pp. 508–518, Mar. 1996.

[15] M. A. Westenberg and T. Ertl, "Vector wavelet thresholding for vector field denoising," in *Proc. Conf. IEEE Vis.*, 2004, pp. 25p–25p.

[16] M. A. Westenberg and T. Ertl, "Denoising 2-D vector fields by vector wavelet thresholding," *J. WSCG*, vol. 13, no. 1, pp. 33–40, 2005.

[17] J. Lumley, "The structure of inhomogeneous turbulence," *Atmospheric Turbulence Wave Propag.*, pp. 167–178, 1967.
[18] L. Sirovich, "Turbulence and the dynamics of coherent structures, parts 1–3," *Quarterly App. Math.*, vol. 45, pp. 561–590, 1987.
[19] G. Berkooz, P. Holmes, and J. Lumley, "The proper orthogonal decomposition in the analysis of turbulent flows," *Annu. Rev. Fluid Mech.*, vol. 25, pp. 539–575, 1993.
[20] M. Kirby, J. P. Boris, and L. Sirovich, "A proper orthogonal decomposition of a simulated supersonic shear layer," *Int. J. Num. Meth. Fluids*, vol. 10, no. 4, pp. 411–428, 1993.
[21] K. E. Meyer, J. M. Pederson, and O. Özcan, "A turbulent jet in crossflow analysed with proper orthogonal decomposition," *J. Fluid Mech.*, vol. 583, pp. 199–227, 2007.
[22] J. Hunt, "Vorticity and vortex dynamics in complex turbulent flows," *Trans. Canadian Society Mech. Eng.*, vol. 11, no. 1, pp. 21–35, 1987.
[23] M. S. Chong, A. E. Perry, and B. J. Cantwell, "A general classification of three-dimensional flow fields," *Phys. Fluids A*, vol. 2, no. 5, pp. 765–777, 1990.
[24] J. Jeong and F. Hussain, "On the identification of a vortex," *J. Fluid Mech.*, vol. 285, pp. 69–94, 1995.
[25] J. Sahner, T. Weinkauf, and H.-C. Hege, "Galilean invariant extraction and iconic representation of vortex core lines," in *Proc. Eurographics/IEEE VGTC Symp. Vis.*, 2005, pp. 151–160.
[26] J. Kasten, J. Reininghaus, I. Hotz, and H.-C. Hege, "Two-dimensional time-dependent vortex regions based on the acceleration magnitude," *IEEE Trans. Vis. Comput. Graph.*, vol. 17, no. 12, pp. 2080–2087, Dec. 2011.
[27] A. Pobitzer *et al.*., "On the way towards topology-based visualization of unsteady flow - the state of the art," in *Proc. EuroGraphics State Art Reports*, 2010.
[28] T. Günther, M. Schulze, and H. Theisel, "Rotation invariant vortices for flow visualization," *IEEE Trans. Vis. Comput. Graph.*, vol. 22, no. 1, pp. 817–826, Jan. 2016.
[29] T. Günther, M. Gross, and H. Theisel, "Generic objective vortices for flow visualization," *ACM Trans. Graph.*, vol. 36, no. 4, pp. 141:1–141:11, 2017.
[30] A. Agranovsky, D. Camp, C. Garth, E. W. Bethel, K. I. Joy, and H. Childs, "Improved post hoc flow analysis via Lagrangian representations," in *Proc. IEEE Symp. Large Data Anal. Vis.*, 2014, pp. 67–75.
[31] G. Arfken, *Mathematical Methods for Physicists*, 3rd ed., New York, NY, USA: Academic, 1985.
[32] H. Margenau and G. M. Murphy, *The Mathematics of Physics and Chemisty*. Princeton, NJ, USA: D Van Nostrand Company, Inc, 1943.
[33] H. Helmholtz, "On integrals of the hydrodynamical equations, which express vortex-motion," *Philos. Magazine J. Sci.*, vol. 33, no. 226, pp. 485–512, 1867.
[34] A. J. Chorin and J. E. Marsden, *A Mathematical Introduction to Fluid Mechanics*. Berlin, Germany: Springer, 1993.
[35] H. Bhatia, G. Norgard, V. Pascucci, and P.-T. Bremer, "The Helmholtz-Hodge decomposition – A survey," *IEEE Trans. Vis. Comput. Graph.*, vol. 19, no. 8, pp. 1386–1404, Aug. 2013.
[36] K. Polthier and E. Preuß, "Identifying vector field singularities using a discrete Hodge decomposition," in *Proc. Math. Vis. III*, 2003, pp. 112–134.
[37] A. Wiebel, "Feature detection in vector fields using the Helmholtz-Hodge decomposition," Diplomarbeit, Univ. Kaiserslautern, Kaiserslautern, Germany, 2004.
[38] R. W. Grout *et al.*"A direct numerical simulation study of turbulence and flame structure in transverse jets analysed in jet-trajectory based coordinates," *J. Fluid Mech.*, vol. 706, pp. 351–383, 2012.
[39] C. S. Yoo, E. S. Richardson, R. Sankaran, and J. H. Chen, "A DNS study on the stabilization mechanism of a turbulent lifted ethylene jet flame in highly-heated coflow," *Proc. Combustion Institute*, vol. 33, no. 1, pp. 1619–1627, 2011.
[40] G. L. Kindlmann, R. S. J. Estepar, S. M. Smith, and C.-F. Westin, "Sampling and visualizing creases with scale-space particles," *IEEE Trans. Vis. Comput. Graph.*, vol. 15, no. 6, pp. 1415–1424, Nov. 2009.
[41] H. Bhatia, A. Gyulassy, H. Wang, P.-T. Bremer, and V. Pascucci, "Robust detection of singularities in vector fields," in *Topological Methods in Data Analysis and Visualization III*, P.-T. Bremer, I. Hotz, V. Pascucci, and R. Peikert, Eds. Berlin, Germany: Springer, 2014, pp. 3–18.
[42] M. Frigo and S. G. Johnson, "The design and implementation of fftw3," *Proc. IEEE*, vol. 93, no. 2, pp. 216–231, Feb 2005.
[43] A. Wiebel, C. Garth, and G. Scheuermann, "Localized flow analysis of 2D and 3D vector fields," in *Proc. 7th Joint Eurographics / IEEE VGTC Conf. Vis.*, 2005, pp. 143–150.

Harsh Bhatia received the PhD degree in scientific computing & imaging institute from the University of Utah, in 2015. He is currently a computer scientist at the Center for Applied Scientific Computing at Lawrence Livermore National Laboratory. His research spans the broad area of visualization and computational topology, with special focus on scientific data. He is also interested in ML-based approaches for scientific applications. Prior to joining LLNL, where he worked on the feature extraction for vector fields.

Robert M. Kirby (Senior Member, IEEE) received the MS and PhD degrees in applied mathematics, and the MS degree in computer science from Brown University, Providence, in 1999, 2002, and 2001, respectively. He is currently the executive director of the Utah Informatics Initiative (UI2), the Interim director of the Scientific Computing and Imaging (SCI) Institute, and a professor of Computing and the associate director of the School of Computing, University of Utah, Salt Lake City. His current research interests include scientific and data computing and visualization.

Valerio Pascucci is the Inaugural John R. Parks Endowed Chair of the University of Utah and the founding Director of the Center for Extreme Data Management Analysis and Visualization (CEDMAV) of the University of Utah. He is also a faculty of the Scientific Computing and Imaging Institute, a professor of the School of Computing, University of Utah, and a Laboratory Fellow, of PNNL and a visiting professor in KAUST. Before joining the University of Utah, Valerio was the Data Analysis Group Leader of the Center for Applied Scientific Computing at Lawrence Livermore National Laboratory, and an adjunct professor of Computer Science at the University of California Davis. His research interests include Big Data management and analytics, progressive multi-resolution techniques in scientific visualization, discrete topology, geometric compression, computer graphics, computational geometry, geometric programming, and solid modeling.

Peer-Timo Bremer received the PhD degree in computer science from the University of California, Davis in 2004, and the diploma degree in mathematics and computer science from the Leibniz University in Hannover, Germany, in 2000. He is currently a member of technical staff and project leader at the Center for Applied Scientific Computing (CASC) at the Lawrence Livermore National Laboratory (LLNL) and associated director for research at the Center for Extreme Data Management, Analysis, and Visualization at the University of Utah. His research interests include large scale data analysis, performance analysis and visualization and he recently coorganized a Dagstuhl Perspectives workshop on integrating performance analysis and visualization. Prior to his tenure at CASC, he was a postdoctoral research associate at the University of Illinois, Urbana-Champaign. He is a member of the IEEE Computer Society and ACM.